SUPPLEMENTARY INFORMATION

Novel B(Ar')$_2$(Ar'') hetero-tri(aryl)boranes: a systematic study of Lewis acidity

Robin J. Blagg,* Trevor R. Simmons, Georgina R. Hatton, James M. Courtney, Elliot L. Bennett, Elliot J. Lawrence and Gregory G. Wildgoose*

School of Chemistry, University of East Anglia, Norwich, NR4 7TJ, U.K.

* *g.wildgoose@uea.ac.uk* ; *r.blagg@uea.ac.uk*

Experimental

B{3,5-(CF$_3$)$_2$C$_6$H$_3$}$_2$(OH)

^{1}H NMR (500.21 MHz, CD_2Cl_2, 25 ºC, δ): +8.20 (s, 4H, Ar^{F6} 2,6-H), +8.10 (s, 2H, Ar^{F6} 4-H), +6.61 (s, 1H, OH); ^{11}B NMR (160.49 MHz, CD_2Cl_2, 25 ºC, δ): +44.3 (br.s); ^{13}C{^{1}H} NMR (125.78 MHz, CD_2Cl_2, 25 ºC, δ): +134.9 (br.q, $^3J_{CF}$ = 3.7 Hz, Ar^{F6} 2,6-C), +131.9 (q, $^2J_{CF}$ = 33.0 Hz, Ar^{F6} 3,5-C), +125.8 (sept., $^3J_{CF}$ = 3.7 Hz, Ar^{F6} 4-C), +124.0 (q, $^1J_{CF}$ = 273 Hz, Ar^{F6} 3,5-CF_3); ^{19}F NMR (470.67 MHz, CD_2Cl_2, 25 ºC, δ): −63.4 (s, 12F, Ar^{F6} 3,5-CF_3).

B{3,5-(CF$_3$)$_2$C$_6$H$_3$}(OMe)$_2$

^{1}H NMR (500.21 MHz, C_6D_6, 25 ºC, δ): +7.86 (s, 2H, Ar^{F6} 2,6-H), +7.79 (s, 1H, Ar^{F6} 4-H), +3.30 (s, 6H, OMe); ^{11}B NMR (160.49 MHz, C_6D_6, 25 ºC, δ): +27.2 (br.s); ^{19}F NMR (470.67 MHz, C_6D_6, 25 ºC, δ): −62.7 (s, 6F, Ar^{F6} 3,5-CF_3).

SUPPLEMENTARY INFORMATION

X-ray Crystallography

To ensure the refinement of **6** converged it was necessary to treat the boron atom as isotropic. Additionally one of the CF_3 groups is modelled with crystallographic disorder of the fluoride atoms over two positions (58:42) due to rotation about the C(17)–C(20)F_3 bond.

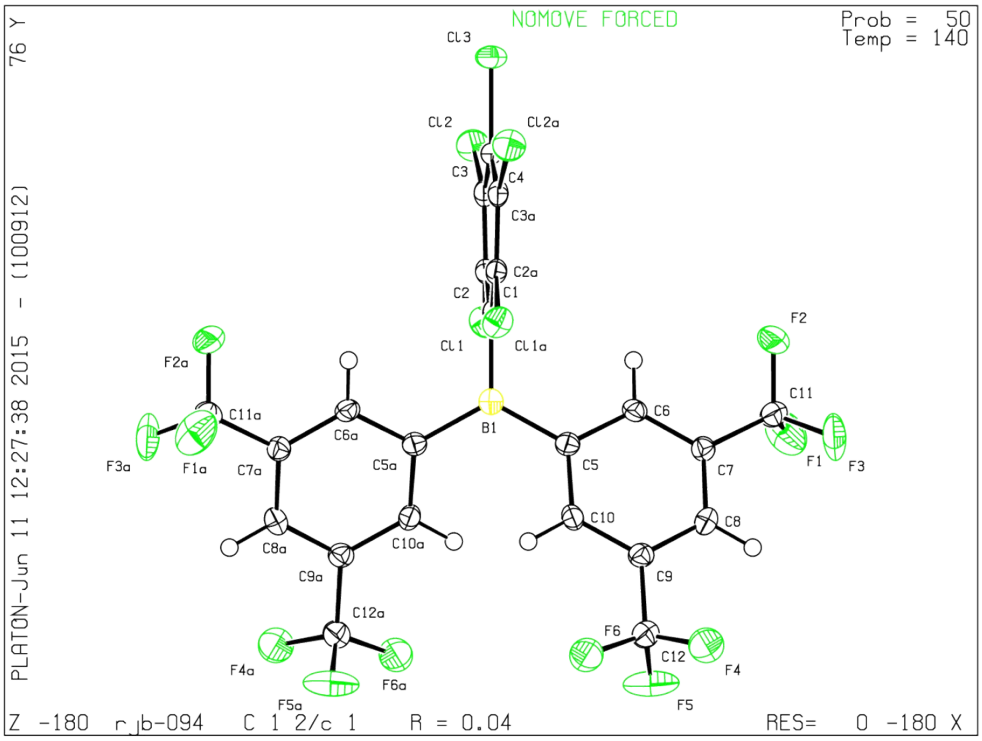

Figure S1a *X*-ray crystallographic structure of B{3,5-$(CF_3)_2C_6H_3$}$_2$(C_6Cl_5) **5**

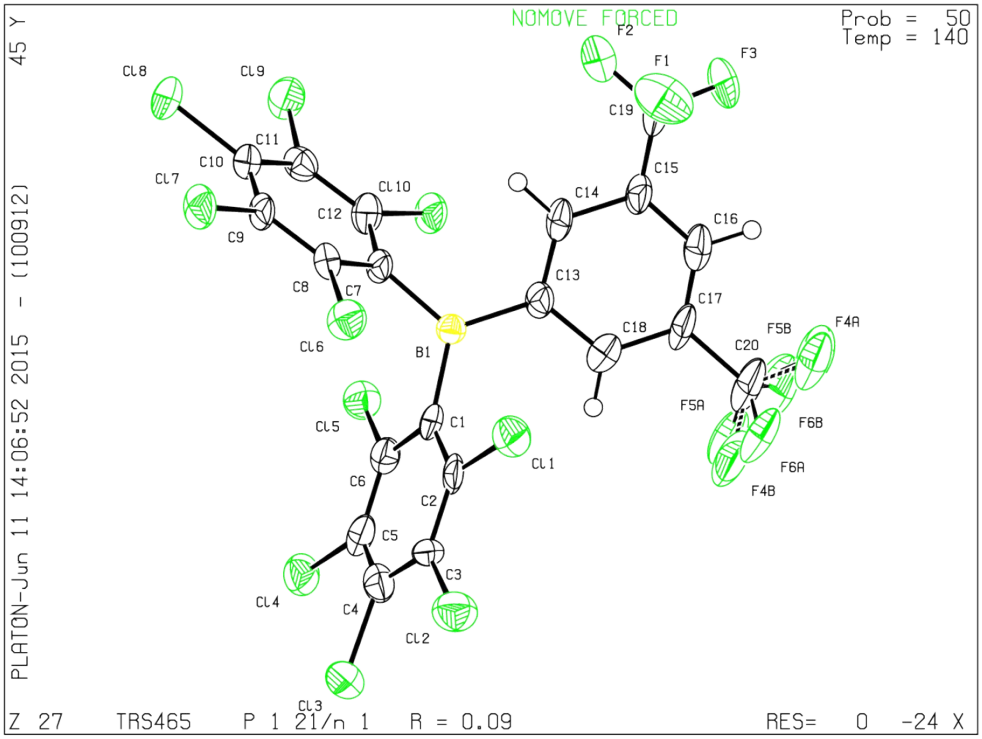

Figure S1b *X*-ray crystallographic structure of B(C_6Cl_5)$_2${3,5-$(CF_3)_2C_6H_3$} **6**

SUPPLEMENTARY INFORMATION

Computational Calculations – DFT

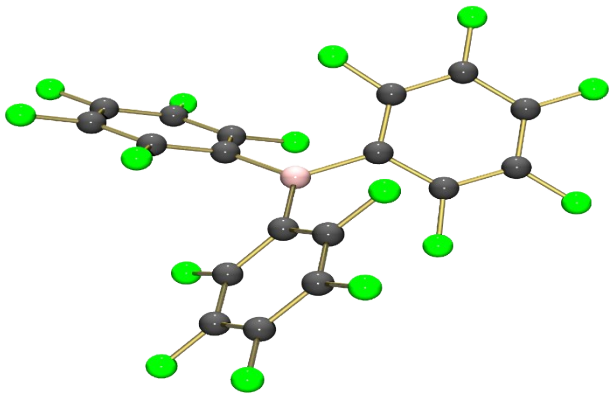

Figure S2a DFT optimised structure of $B(C_6F_5)_3$ **1** (reproduced from reference 34)

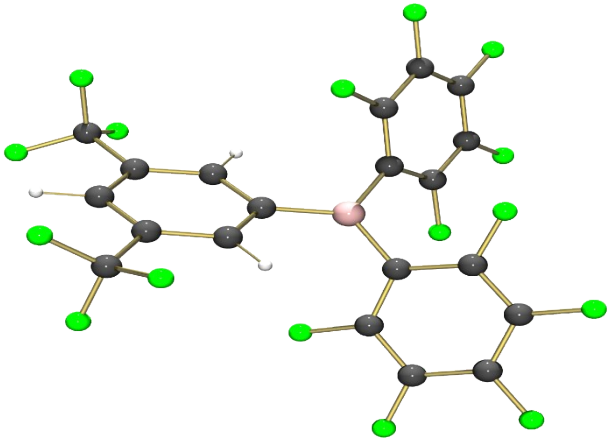

Figure S2b DFT optimised structure of $B(C_6F_5)_2\{3,5\text{-}(CF_3)_2C_6H_3\}$ **2**

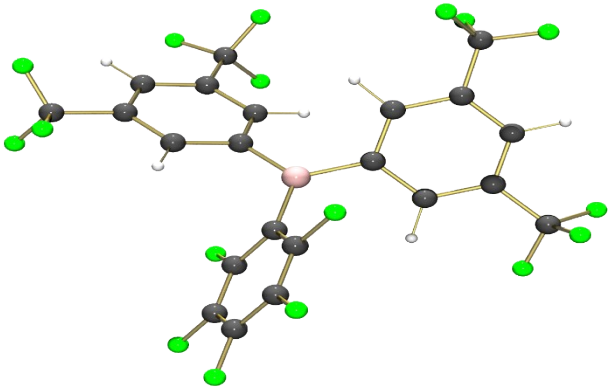

Figure S2c DFT optimised structure of $B\{3,5\text{-}(CF_3)_2C_6H_3\}_2(C_6F_5)$ **3**

SUPPLEMENTARY INFORMATION

Computational calculations were performed using density functional theory (DFT) using the Gaussian 09 (revision C.01) computational package.[S1] Calculations were carried out using the three-parameter exchange functional of Becke (B3) with the correlation functional of Lee, Yang, and Parr (LYP), B3LYP;[S2, S3] together with applying the 6-311+G(d,p) basis set for all atoms.[S4] Structures were geometry optimised in the gas phase with the default convergence criteria, and confirmed as minima through frequency calculations.

[S1] *Gaussian 09, Revision C.01*, M. J. Frisch, G. W. Trucks, H. B. Schlegel, G. E. Scuseria, M. A. Robb, J. R. Cheeseman, G. Scalmani, V. Barone, B. Mennucci, G. A. Petersson, H. Nakatsuji, M. Caricato, X. Li, H. P. Hratchian, A. F. Izmaylov, J. Bloino, G. Zheng, J. L. Sonnenberg, M. Hada, M. Ehara, K. Toyota, R. Fukuda, J. Hasegawa, M. Ishida, T. Nakajima, Y. Honda, O. Kitao, H. Nakai, T. Vreven, J. A. Montgomery, Jr., J. E. Peralta, F. Ogliaro, M. Bearpark, J. J. Heyd, E. Brothers, K. N. Kudin, V. N. Staroverov, T. Keith, R. Kobayashi, J. Normand, K. Raghavachari, A. Rendell, J. C. Burant, S. S. Iyengar, J. Tomasi, M. Cossi, N. Rega, J. M. Millam, M. Klene, J. E. Knox, J. B. Cross, V. Bakken, C. Adamo, J. Jaramillo, R. Gomperts, R. E. Stratmann, O. Yazyev, A. J. Austin, R. Cammi, C. Pomelli, J. W. Ochterski, R. L. Martin, K. Morokuma, V. G. Zakrzewski, G. A. Voth, P. Salvador, J. J. Dannenberg, S. Dapprich, A. D. Daniels, O. Farkas, J. B. Foresman, J. V. Ortiz, J. Cioslowski, and D. J. Fox, Gaussian, Inc., Wallingford CT, 2010.

[S2] A. D. Becke, *J. Chem. Phys.*, 1993, **98**, 5648-5652.

[S3] C. Lee, W. Yang and R. G. Parr, *Phys. Rev. B Condens. Matter*, 1988, **37**, 785-789.

[S4] P. C. Hariharan and J. A. Pople, *Theor. Chim. Acta.*, 1973, **28**, 213-222.

SUPPLEMENTARY INFORMATION

Electrochemical Studies

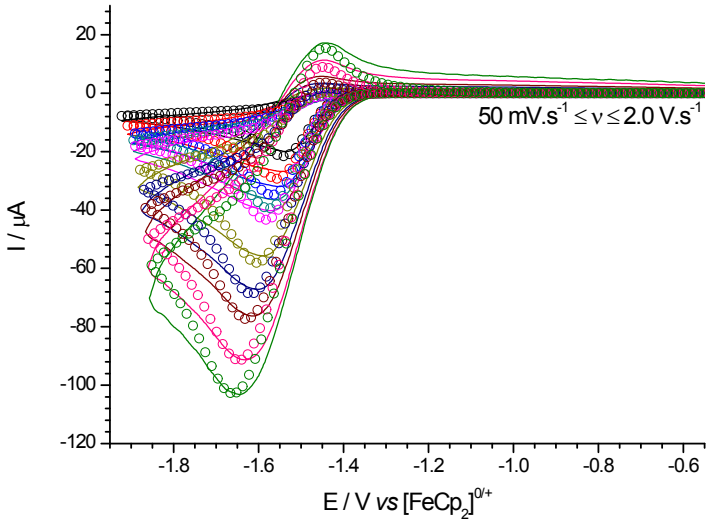

Figure S3a Experimental (line) and simulated (open circles) cyclic voltammograms for the reduction of $B(C_6F_5)_3$ **1** (reproduced from reference 37)

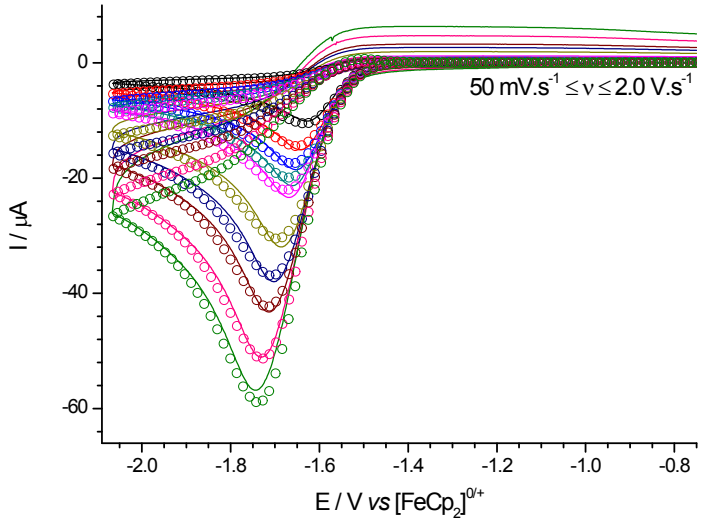

Figure S3b Experimental (line) and simulated (open circles) cyclic voltammograms for the reduction of $B\{3,5\text{-}(CF_3)_2C_6H_3\}_3$ **4** (reproduced from reference 37)

SUPPLEMENTARY INFORMATION

Cyclic voltammograms were also obtained of a pure sample of B{3,5-$(CF_3)_2C_6H_3$}$_2$(OH), showing a one electron irreversible reduction at considerably more negative potentials (*ca.* −2.3 V *vs* $[FeCp_2]^{0/+}$) than observed for any of the tri(aryl)boranes (Figure S4).

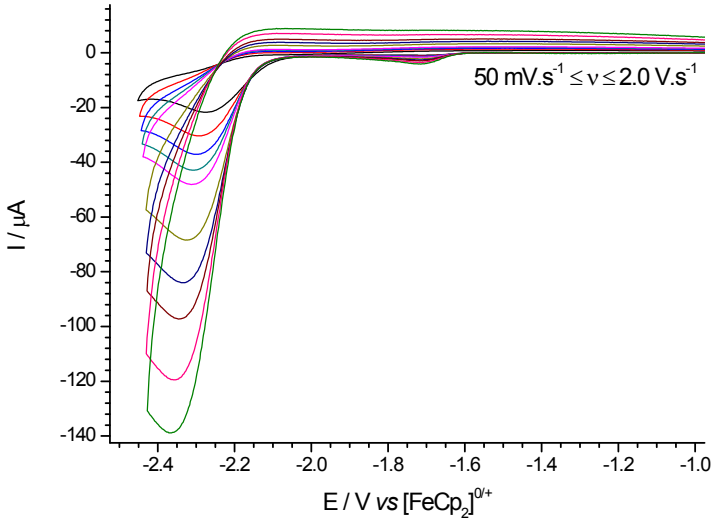

Figure S4 Experimental cyclic voltammograms for the reduction of B{3,5-$(CF_3)_2C_6H_3$}$_2$(OH)

SUPPLEMENTARY INFORMATION

Measurements of Lewis acidity

"Gutmann-Beckett Method" $B(Ar')_2(Ar'')$ (Lewis acid) is combined with a three-fold excess of $OPEt_3$ (Lewis base) in *ca.* 0.8 cm^3 CD_2Cl_2 in an NMR tube, rapidly generating the Lewis acid-base adduct $Et_3POB(Ar')_2(Ar'')$, and ^1H, ^{11}B, ^{19}F and $^{31}P\{^1H\}$ NMR spectra obtained (Tables 3 & S1).

Table S1 NMR spectral data for the Lewis acid/base adducts **1**−$OPEt_3$ – **9**−$OPEt_3$

1−$OPEt_3$	^1H NMR (500.21 MHz, CD_2Cl_2, 25 ºC, δ): +1.92 (dq $^4J_{HP}$ = 12.2 Hz, $^3J_{HH}$ = 7.7 Hz, 6H), +1.11 (dt, $^3J_{HP}$ = 18.7 Hz, $^3J_{HH}$ = 7.7 Hz, 9H); ^{19}F NMR (470.67 MHz, CD_2Cl_2, 25 ºC, δ): −134.4 (m, 6F), −159.1 (t, $^3J_{FF}$ = 19.9 Hz, 3F), −165.0 (m, 6F).
2−$OPEt_3$	^1H NMR (500.21 MHz, CD_2Cl_2, 25 ºC, δ): +7.79 (s, 2H), +7.68 (s 1H), +1.86 (dq, $^4J_{HP}$ = 12.0 Hz, $^3J_{HH}$ = 7.8 Hz, 6H); ^{19}F NMR (470.67 MHz, CD_2Cl_2, 25 ºC, δ): −62.9 (s, 6F), −132.0 (m, 4F), −158.5 (t, $^3J_{FF}$ = 19.9 Hz, 2F), −164.1 (m, 4F).
3−$OPEt_3$	^1H NMR (500.21 MHz, CD_2Cl_2, 25 ºC, δ): +7.83 (s, 4H), +7.78 (s 2H), +1.68 (dq, $^4J_{HP}$ = 11.9 Hz, $^3J_{HH}$ = 7.6 Hz, 6H), +1.11 (dt, $^3J_{HP}$ = 18.4 Hz, $^3J_{HH}$ = 7.6 Hz, 9H); ^{19}F NMR (470.67 MHz, CD_2Cl_2, 25 ºC, δ): −63.1 (s, 12F), −131.8 (m, 2F), −158.9 (t, $^3J_{FF}$ = 19.9 Hz, 1F), −163.9 (m, 2F).
4−$OPEt_3$	^1H NMR (500.21 MHz, CD_2Cl_2, 25 ºC, δ): +7.79 (s, 6H), +7.74 (s 3H), +1.68 (dq, $^4J_{HP}$ = 11.9 Hz, $^3J_{HH}$ = 7.7 Hz, 6H), +1.10 (dt, $^3J_{HP}$ = 18.2 Hz, $^3J_{HH}$ = 7.7 Hz, 9H); ^{19}F NMR (470.67 MHz, CD_2Cl_2, 25 ºC, δ): −63.1 (s, 18F).
5−$OPEt_3$	^1H NMR (500.21 MHz, CD_2Cl_2, 25 ºC, δ): +7.90 (s, 4H), +7.75 (s 2H); ^{19}F NMR (470.67 MHz, CD_2Cl_2, 25 ºC, δ): −63.1 (s, 12F).
6−$OPEt_3$	^1H NMR (500.21 MHz, CD_2Cl_2, 25 ºC, δ): +7.94 (s, 2H), +7.65 (s 1H); ^{19}F NMR (470.67 MHz, CD_2Cl_2, 25 ºC, δ): −62.9 (s, 6F).
7−$OPEt_3$	no adduct formation
8−$OPEt_3$	^1H NMR (500.21 MHz, CD_2Cl_2, 25 ºC, δ): +2.00 (br.m, 6H), +1.00 (br.m, 9H); ^{19}F NMR (470.67 MHz, CD_2Cl_2, 25 ºC, δ): −130.0 (br.m, 1F), −133.1 (br.m, 1F), −158.5 (br.m, 1F), −164.0 (br.m, 1F), −165.9 (br.m, 1F).
9−$OPEt_3$	^1H NMR (500.21 MHz, CD_2Cl_2, 25 ºC, δ): +1.96 (dq $^4J_{HP}$ = 12.4 Hz, $^3J_{HH}$ = 7.7 Hz, 6H), +1.02 (dt, $^3J_{HP}$ = 18.8 Hz, $^3J_{HH}$ = 7.7 Hz, 9H);^{19}F NMR (470.67 MHz, CD_2Cl_2, 25 ºC, δ): −133.1 (m, 2F), −158.8 (t, $^3J_{FF}$ = 20.3 Hz, 1F), −164.8 (m, 2F).

If resonances corresponding to the ethyl groups of the adduct are not specified, the resonances are co-incident with / obscured by free Et_3PO: ^1H NMR (500.21 MHz, CD_2Cl_2, 25 ºC, δ): +1.64 (dq $^4J_{HP}$ = 11.7 Hz, $^3J_{HH}$ = 7.7 Hz), +1.11 (dt, $^3J_{HP}$ = 16.1 Hz, $^3J_{HH}$ = 7.7 Hz)

^{11}B NMR (160.49 MHz, CD_2Cl_2, 25 ºC, δ) and $^{31}P\{^1H\}$ NMR (202.49 MHz, CD_2Cl_2, 25 ºC, δ) spectral data reported in Table 3

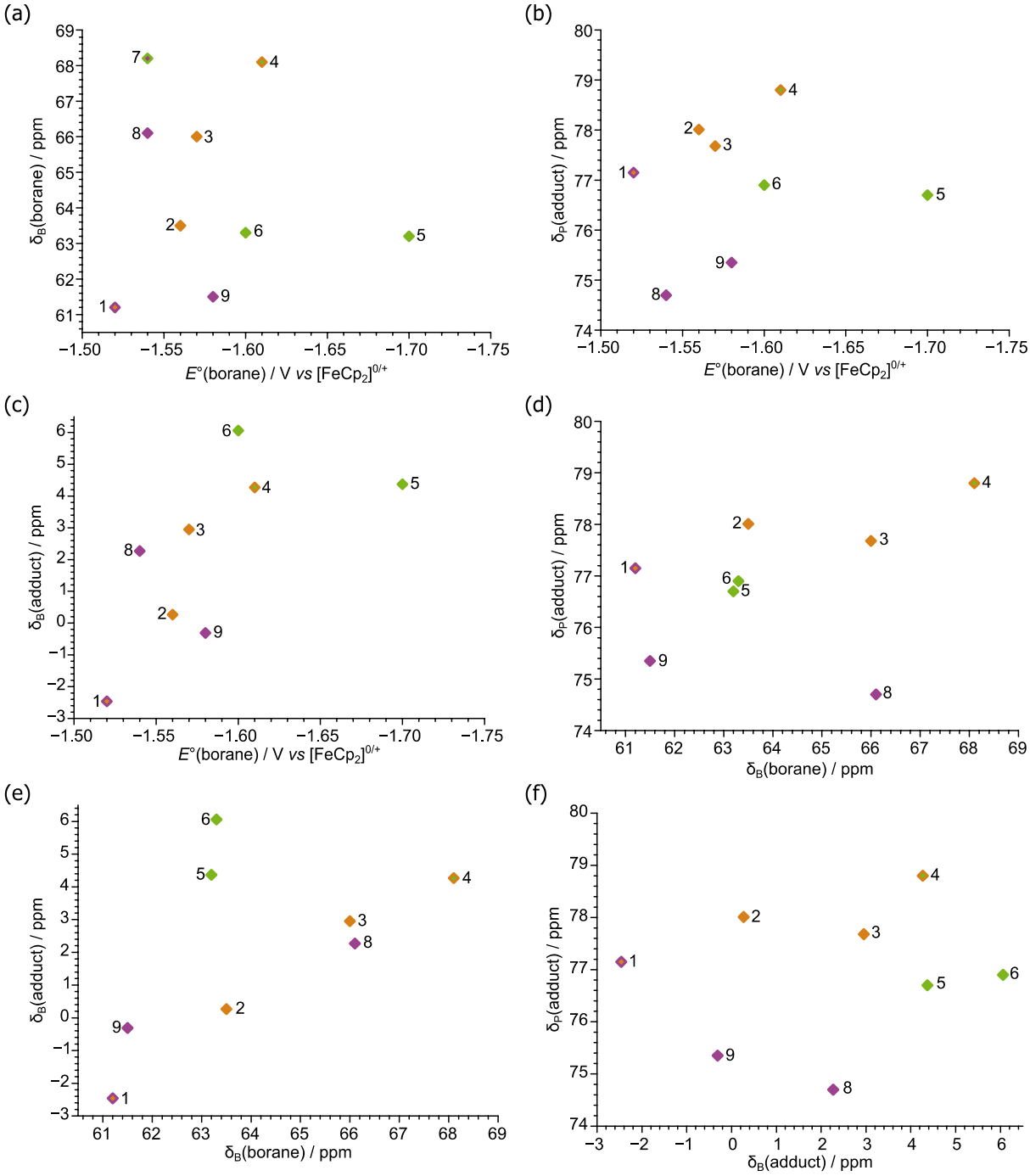

Figure S5 Correlation between: (a) *E*°(borane) and δ_B(borane); (b) *E*°(borane) and δ_P(adduct); (c) *E*°(borane) and δ_B(adduct); (d) δ_B(borane) and δ_P(adduct); (e) δ_B(borane) and δ_B(adduct); (f) δ_P(adduct) and δ_B(adduct).

SUPPLEMENTARY INFORMATION

H_2 cleavage by FLPs

Equimolar quantities of $B(Ar')_2(Ar'')$ (Lewis acid) and $P(^tBu)_3$ (Lewis base) are combined in *ca.* 0.8 cm^3 CD_2Cl_2 (*ca.* 40 mM acid/base concentrations) in an NMR tube fitted with a J.Young valve. ^1H, ^{11}B, ^{19}F and $^{31}P\{^1H\}$ NMR spectra are obtained. The solution is degassed in the NMR tube by three freeze-pump-thaw cycles, before being frozen and the head-space of the NMR tube filled with dry H_2. The NMR tube is allowed to warm to room temperature (giving a H_2 pressure of *ca.* 4 bar), shaken, and the resulting reaction monitored by ^1H and ^{11}B NMR spectroscopy. (Spectra obtained at intervals between 90 min and 12 hours until reaction reaches completion / spectra cease changes). Upon completion of the reaction a final set of ^1H, ^{11}B, ^{19}F and $^{31}P\{^1H\}$ NMR spectra are obtained (data reported in Tables 4 and S2). Reaction mixture was maintained at room temperature (*ca.* +20 °C) throughout.

Table S2 NMR spectral data for the terminal hydride, H_2 cleavage products for the **1**-**9**/$P(^tBu)_3$ FLPs

$[HP(^tBu)_3]^+$	^1H NMR (500.21 MHz, CD_2Cl_2, 25 ºC, δ): +5.12 (d, $^1J_{HP}$ = 430 Hz, 1H), +1.58 (d, $^3J_{HP}$ = 15.7Hz, 27H); $^{31}P\{^1H\}$ NMR (202.49 MHz, CD_2Cl_2, 25 ºC, δ): +59.8 (s).
[H**1**]$^-$	^1H NMR (500.21 MHz, CD_2Cl_2, 25 ºC, δ): +3.60 (br.q, $^1J_{HB}$ = 93.9 Hz, 1H); ^{19}F NMR (470.67 MHz, CD_2Cl_2, 25 ºC, δ): −133.6 (m, 6F), −163.4 (m, 3F), −166.7 (m, 6F).
[H**2**]$^-$	^1H NMR (500.21 MHz, CD_2Cl_2, 25 ºC, δ): +7.68 (s, 2H), +7.48 (s, 1H), +3.69 (br.q, $^1J_{HB}$ = 86.1 Hz, 1H); ^{19}F NMR (470.67 MHz, CD_2Cl_2, 25 ºC, δ): −62.4 (s, 6F), −131.6 (m, 4F), −163.9 (t, $^3J_{FF}$ = 19.9 Hz, 2F), −166.8 (m, 4F).
[H**3**]$^-$	^1H NMR (500.21 MHz, CD_2Cl_2, 25 ºC, δ): +7.74 (s, 4H), +7.51 (s, 2H), +3.71 (br.q, $^1J_{HB}$ = 86.1 Hz, 1H); ^{19}F NMR (470.67 MHz, CD_2Cl_2, 25 ºC, δ): −62.5 (s, 12F), −131.8 (br.m, 2F), −163.6 (t, $^3J_{FF}$ = 19.5 Hz, 1F), −166.0 (m, 2F).
[H**4**]$^-$	no terminal hydride formation
[H**5**]$^-$	^1H NMR (500.21 MHz, CD_2Cl_2, 25 ºC, δ): +7.75 (s, 4H), +7.48 (s, 2H), +4.22 (br.q, $^1J_{HB}$ = 86.1 Hz, 1H); ^{19}F NMR (470.67 MHz, CD_2Cl_2, 25 ºC, δ): −62.5 (s, 12F).
[H**6**]$^-$	^1H NMR (500.21 MHz, CD_2Cl_2, 25 ºC, δ): +7.63 (br.s, 2H), +7.47 (s, 1H), +4.24 (br.q, $^1J_{HB}$ = 88.0 Hz, 1H); ^{19}F NMR (470.67 MHz, CD_2Cl_2, 25 ºC, δ): −62.5 (s, 6F).
[H**7**]$^-$	no reaction
[H**8**]$^-$	^1H NMR (500.21 MHz, CD_2Cl_2, 25 ºC, δ): +4.11 (br.q, $^1J_{HB}$ = 86.1 Hz, 1H); ^{19}F NMR (470.67 MHz, CD_2Cl_2, 25 ºC, δ): −133.9 (m, 4F), −164.8 (m, 2F), −167.7 (m, 4F).
[H**9**]$^-$	^1H NMR (500.21 MHz, CD_2Cl_2, 25 ºC, δ): +3.94 (br.q, $^1J_{HB}$ = 90.0 Hz, 1H); ^{19}F NMR (470.67 MHz, CD_2Cl_2, 25 ºC, δ): −133.5 (m, 4F), −164.9(m, 2F), −167.6 (m, 4F).

^{11}B NMR (160.49 MHz, CD_2Cl_2, 25 ºC, δ) spectral data reported in Table 4

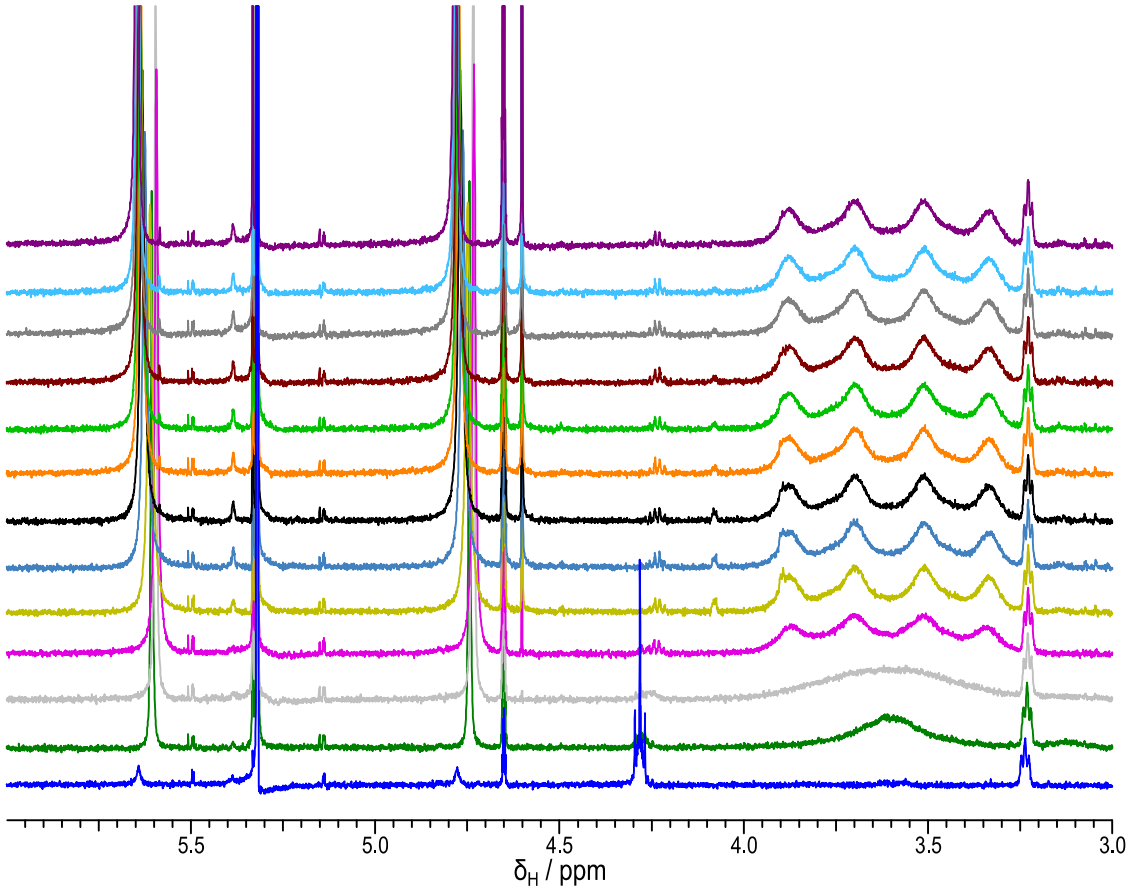

Figure S6a ^{1}H NMR spectra showing the progress of H_2 cleavage by the **1**/P(^{t}Bu)$_3$ FLP post H_2 addition spectra at *ca.* 90 min intervals

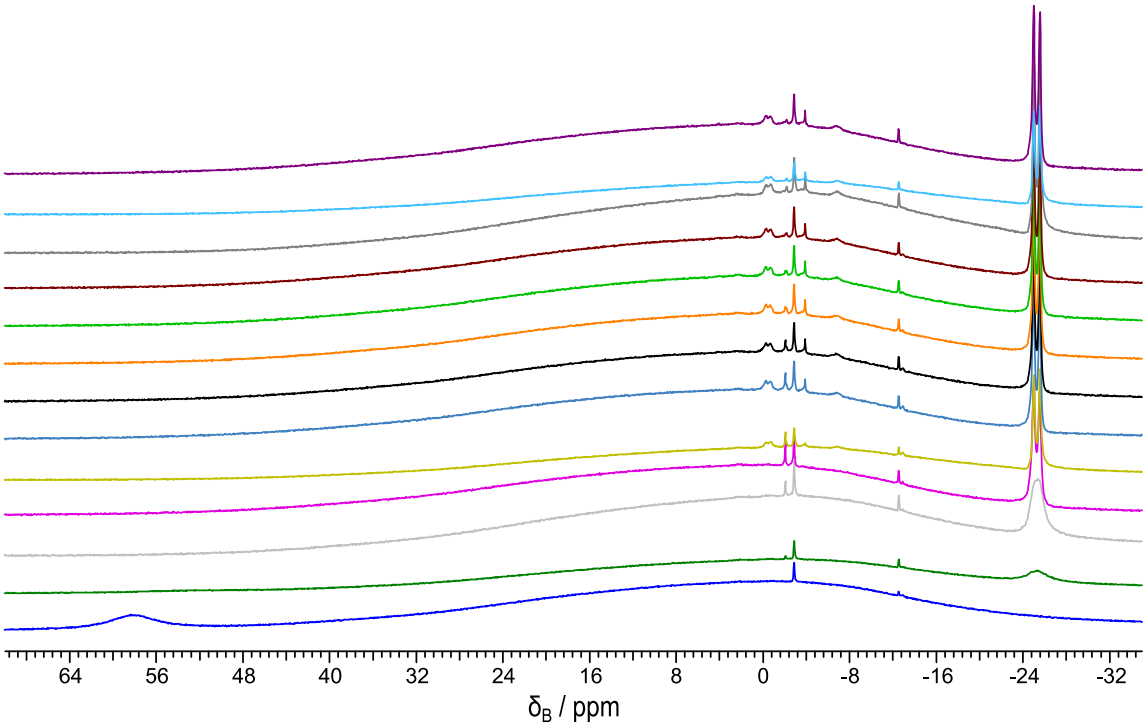

Figure S6b ^{11}B NMR spectra showing the progress of H_2 cleavage by the **1**/P(^{t}Bu)$_3$ FLP post H_2 addition spectra at *ca.* 90 min intervals

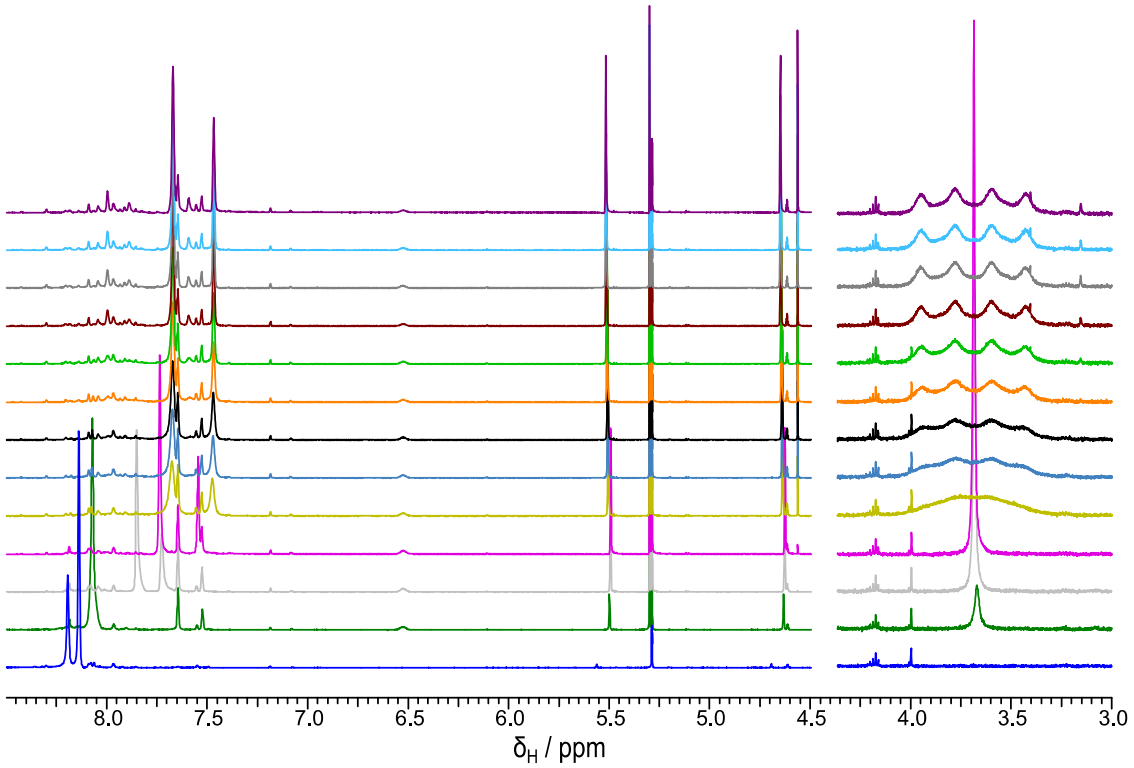

Figure S7a ^{1}H NMR spectra showing the progress of H_2 cleavage by the **2**/P(^{t}Bu)$_3$ FLP post H_2 addition spectra at *ca.* 90 min intervals

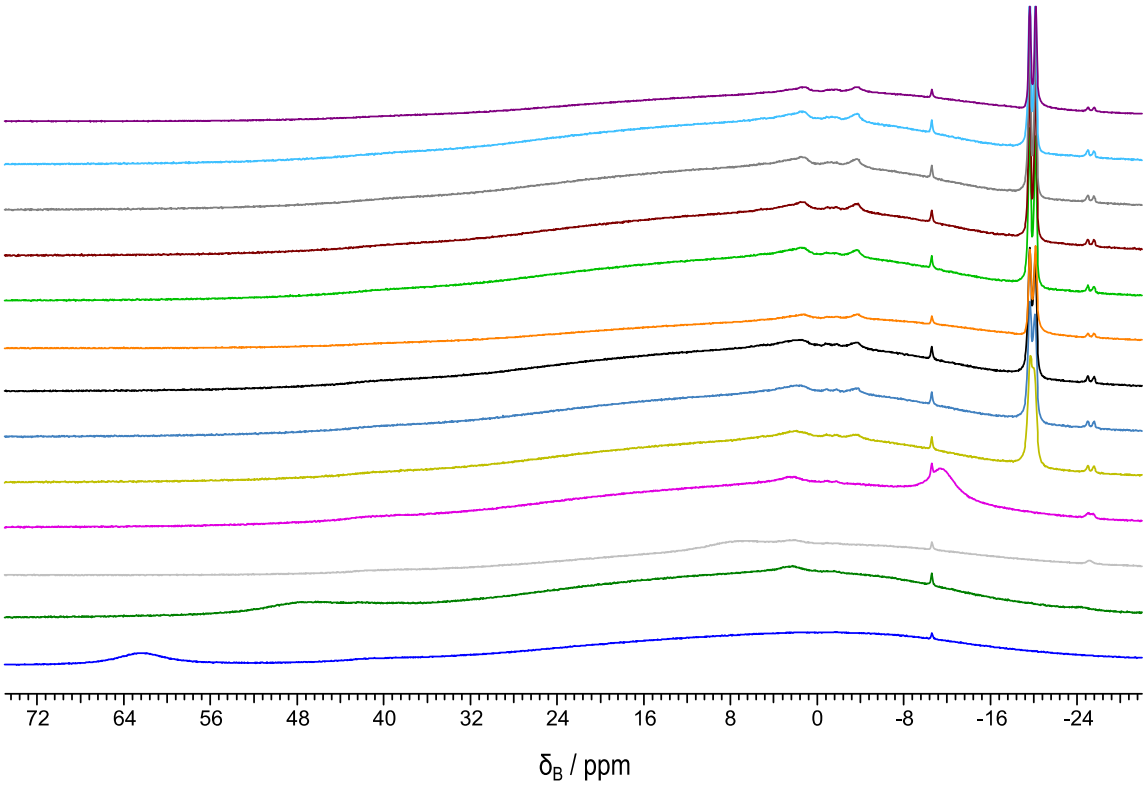

Figure S7b ^{11}B NMR spectra showing the progress of H_2 cleavage by the **2**/P(^{t}Bu)$_3$ FLP post H_2 addition spectra at *ca.* 90 min intervals

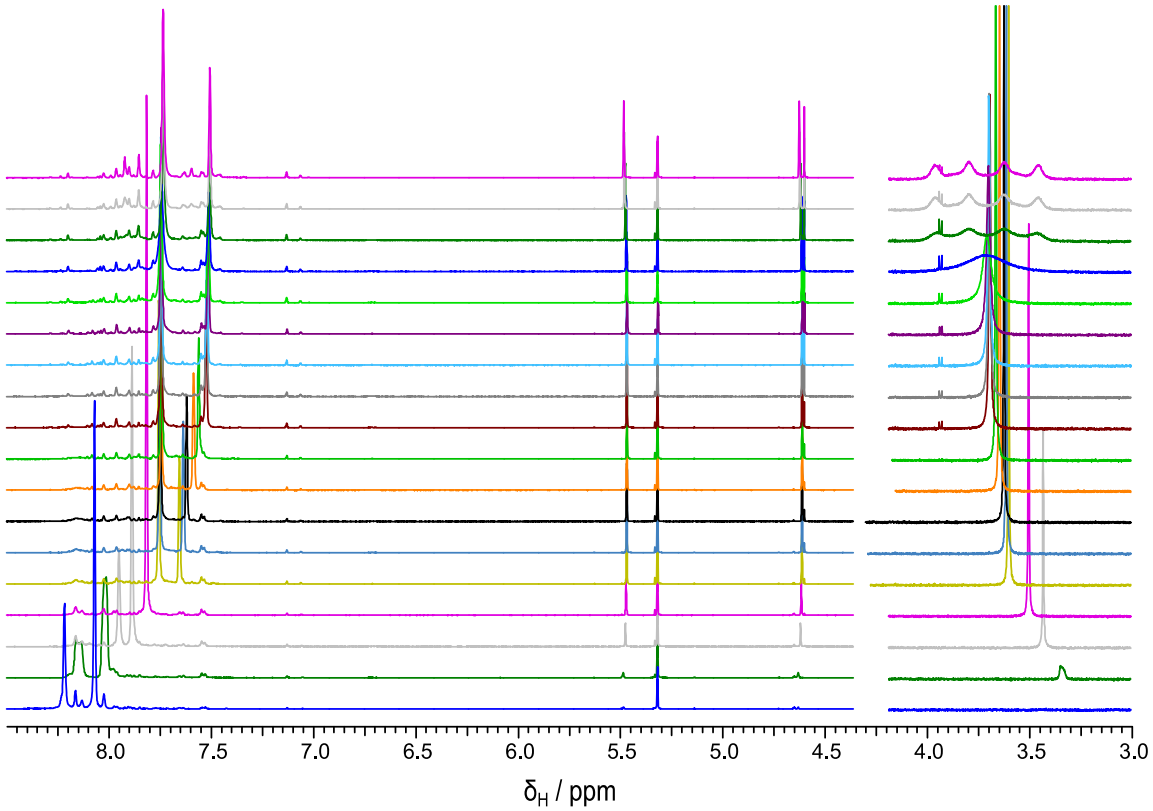

Figure S8a ^{1}H NMR spectra showing the progress of H_2 cleavage by the **3**/P(^{t}Bu)$_3$ FLP post H_2 addition, 12 spectra at *ca.* 90 min intervals, subsequently at *ca.* 12 hour intervals

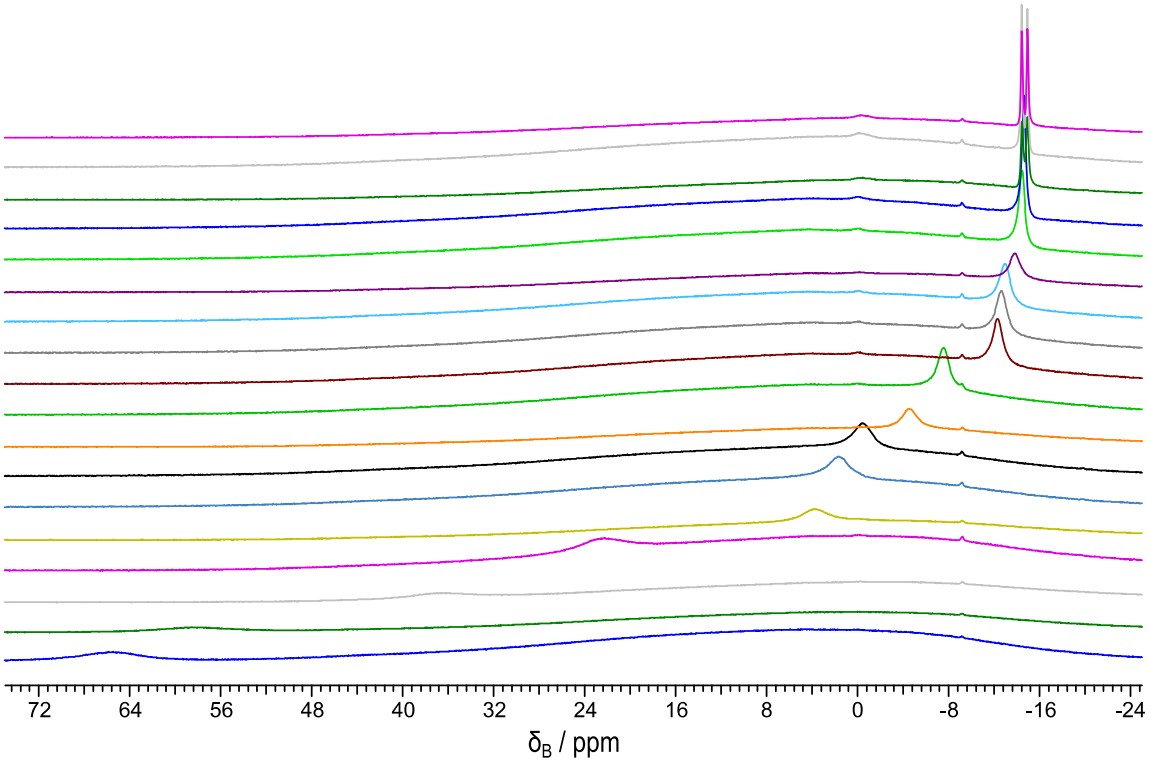

Figure S8b ^{11}B NMR spectra showing the progress of H_2 cleavage by the **3**/P(^{t}Bu)$_3$ FLP post H_2 addition, 12 spectra at *ca.* 90 min intervals, subsequently at *ca.* 12 hour intervals

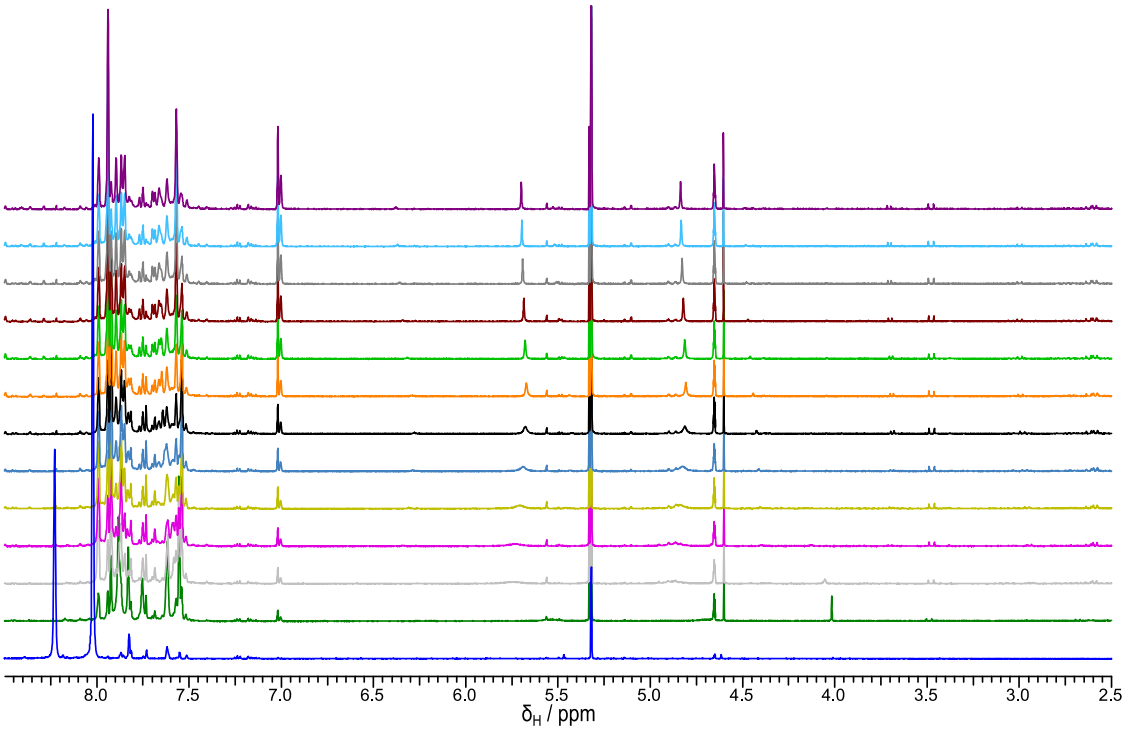

Figure S9a ^{1}H NMR spectra showing the progress of H_2 cleavage by the **4**/P(^{t}Bu)$_3$ FLP post H_2 addition spectra at *ca.* 90 min intervals

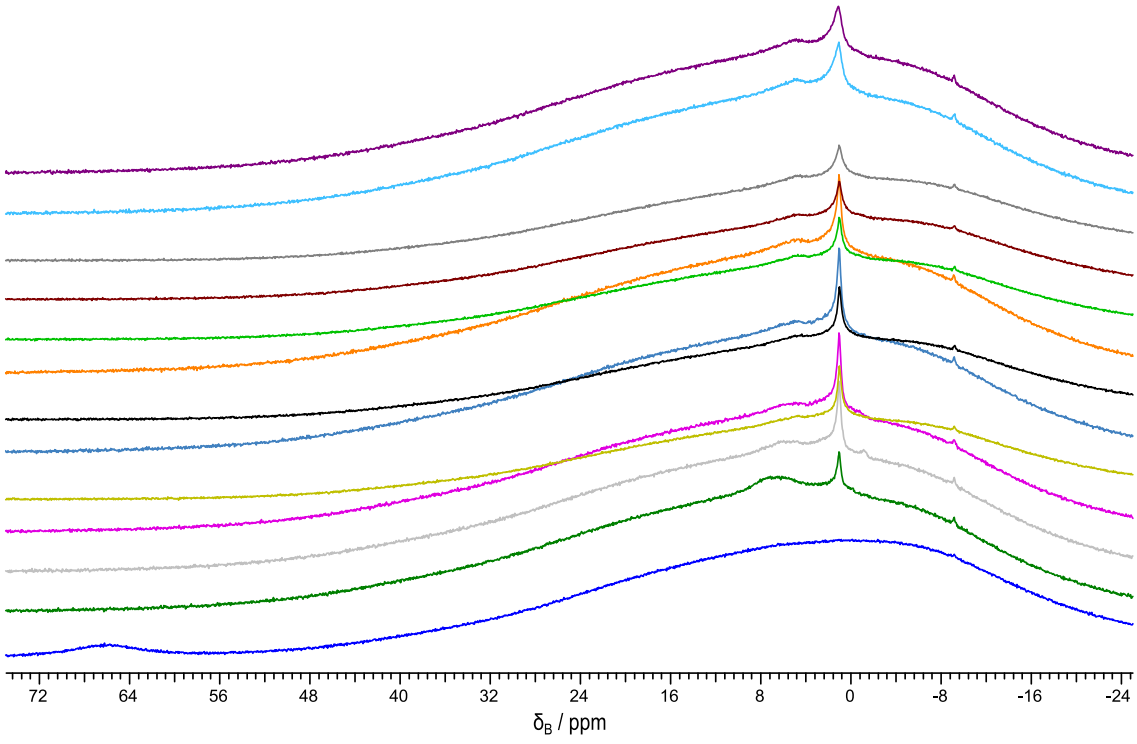

Figure S9b ^{11}B NMR spectra showing the progress of H_2 cleavage by the **4**/P(^{t}Bu)$_3$ FLP post H_2 addition spectra at *ca.* 90 min intervals

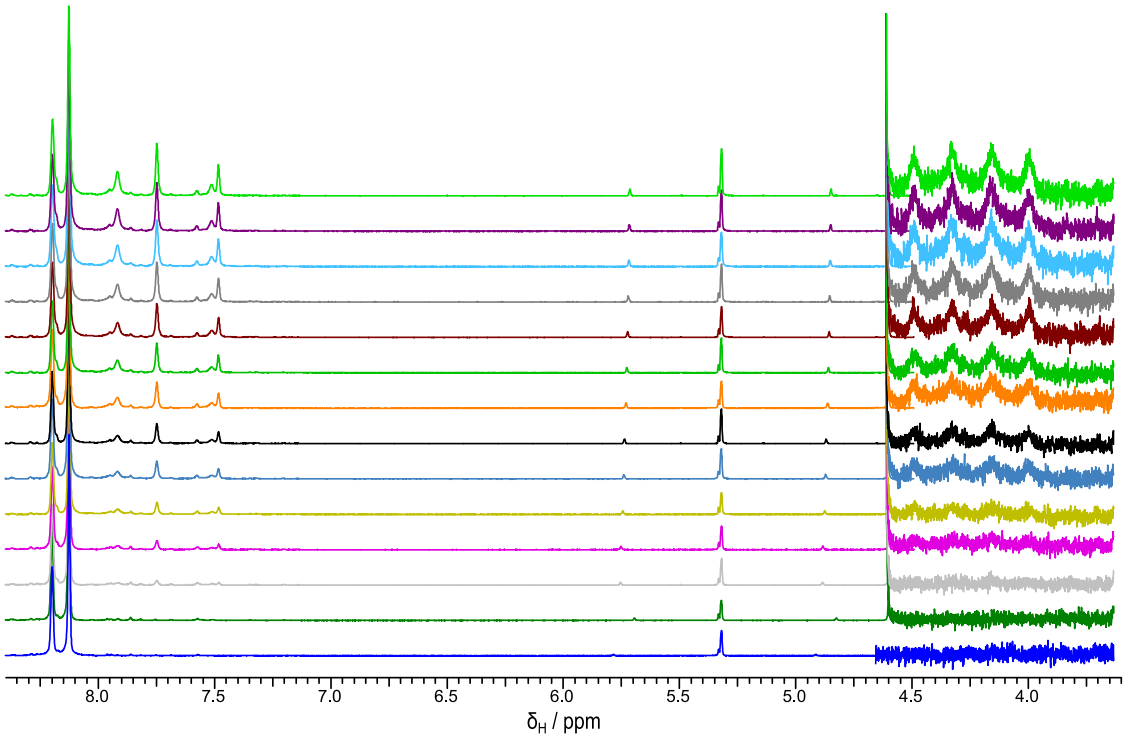

Figure S10a ^{1}H NMR spectra showing the progress of H_2 cleavage by the **5**/P(^{t}Bu)$_3$ FLP post H_2 addition spectra at *ca.* 8 hour intervals

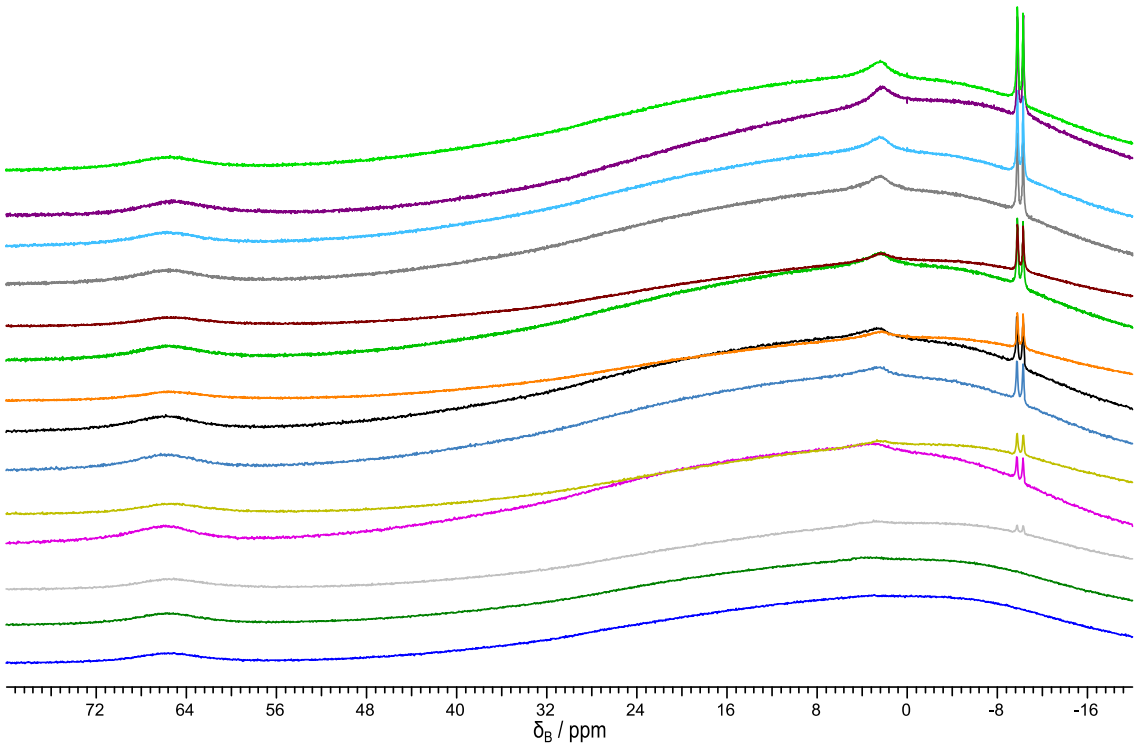

Figure S10b ^{11}B NMR spectra showing the progress of H_2 cleavage by the **5**/P(^{t}Bu)$_3$ FLP post H_2 addition spectra at *ca.* 8 hour intervals

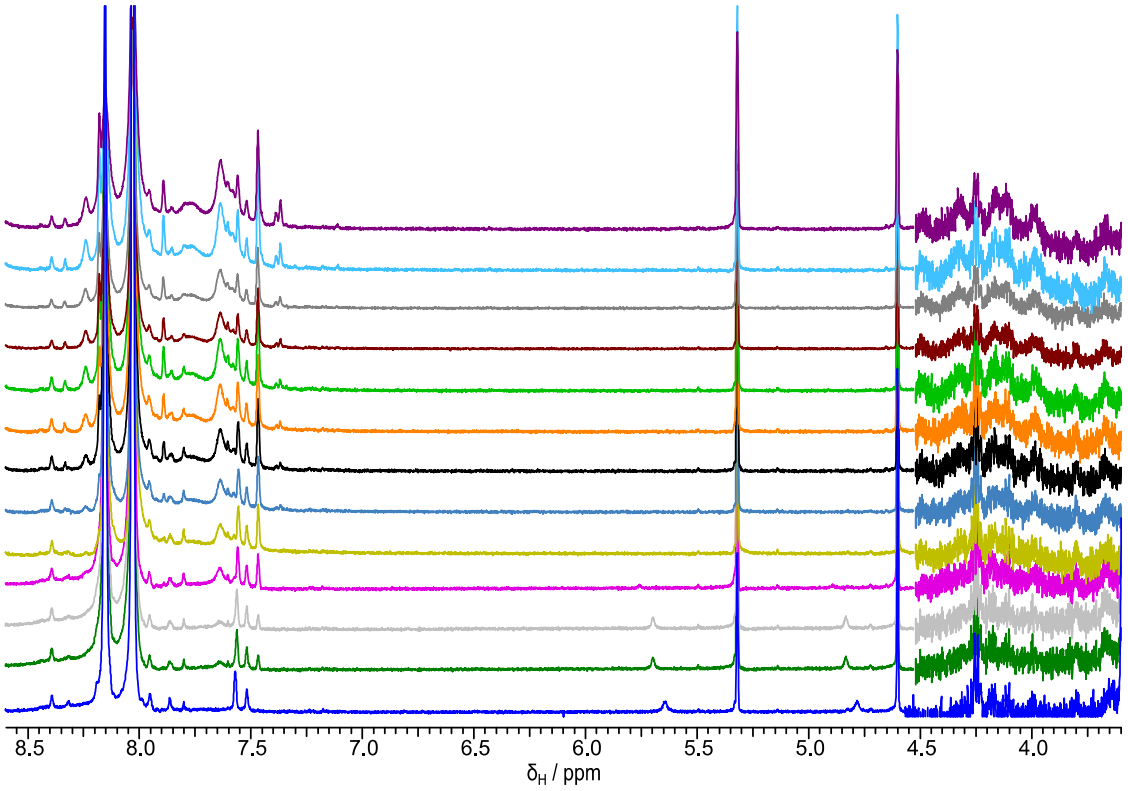

Figure S11a ^{1}H NMR spectra showing the progress of H_2 cleavage by the **6**/P(^{t}Bu)$_3$ FLP post H_2 addition spectra at *ca.* 8 hour intervals

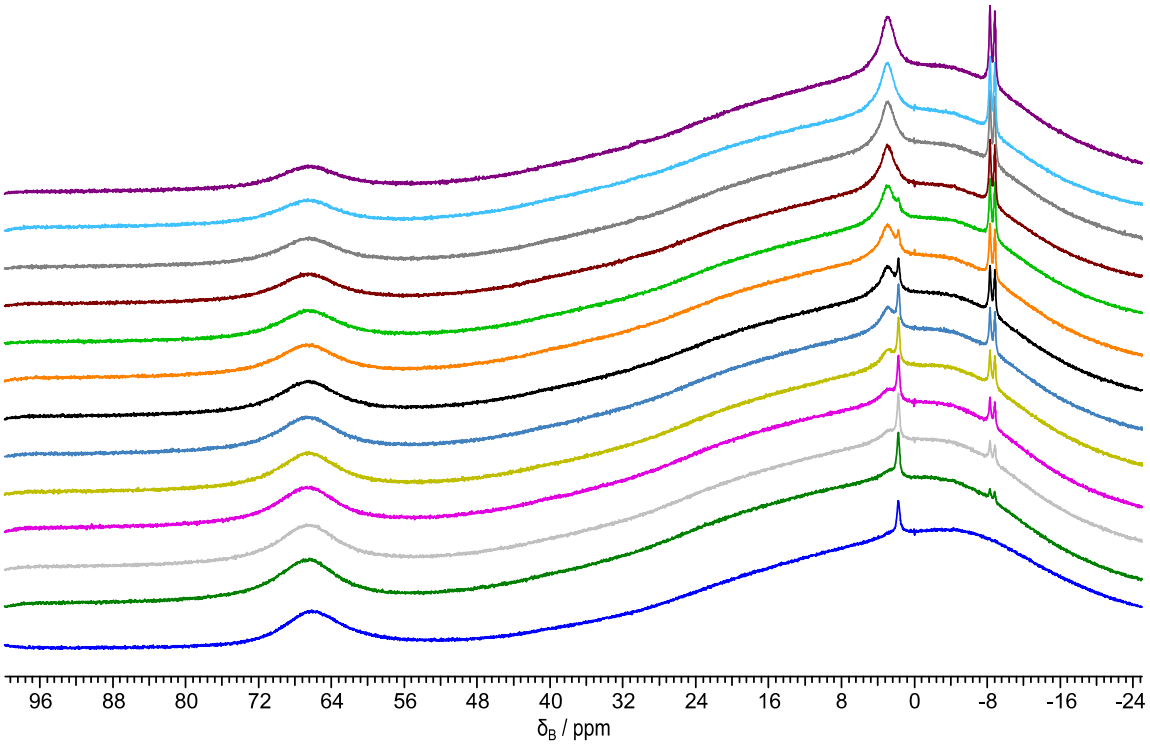

Figure S11b ^{11}B NMR spectra showing the progress of H_2 cleavage by the **6**/P(^{t}Bu)$_3$ FLP post H_2 addition spectra at *ca.* 8 hour intervals

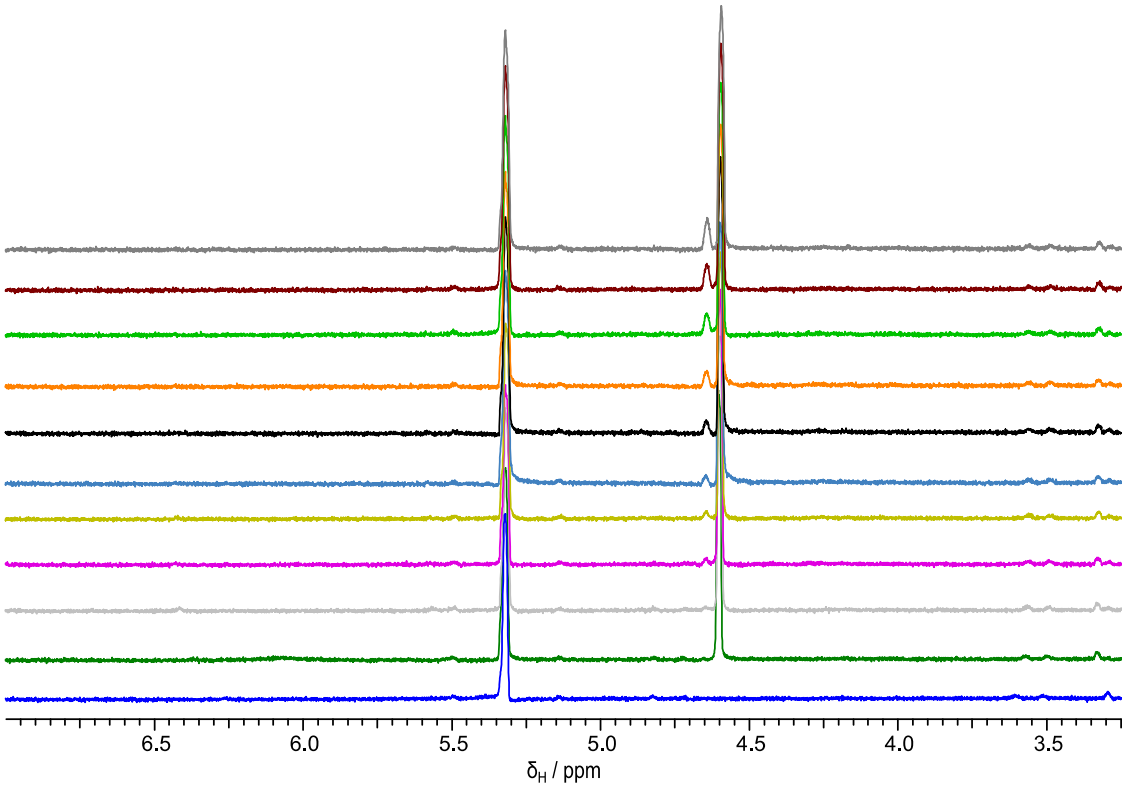

Figure S12a ^{1}H NMR spectra showing the progress of H_2 cleavage by the **7**/P(^{t}Bu)$_3$ FLP post H_2 addition spectra at *ca.* 12 hour intervals

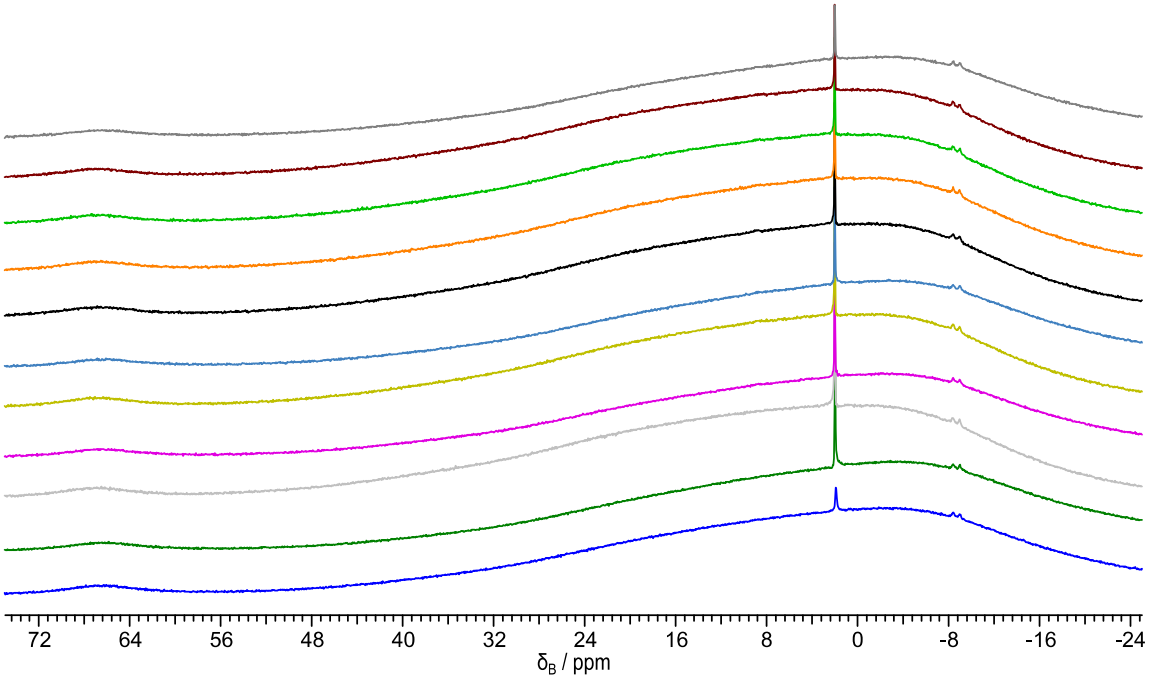

Figure S12b ^{11}B NMR spectra showing the progress of H_2 cleavage by the **7**/P(^{t}Bu)$_3$ FLP post H_2 addition spectra at *ca.* 12 hour intervals

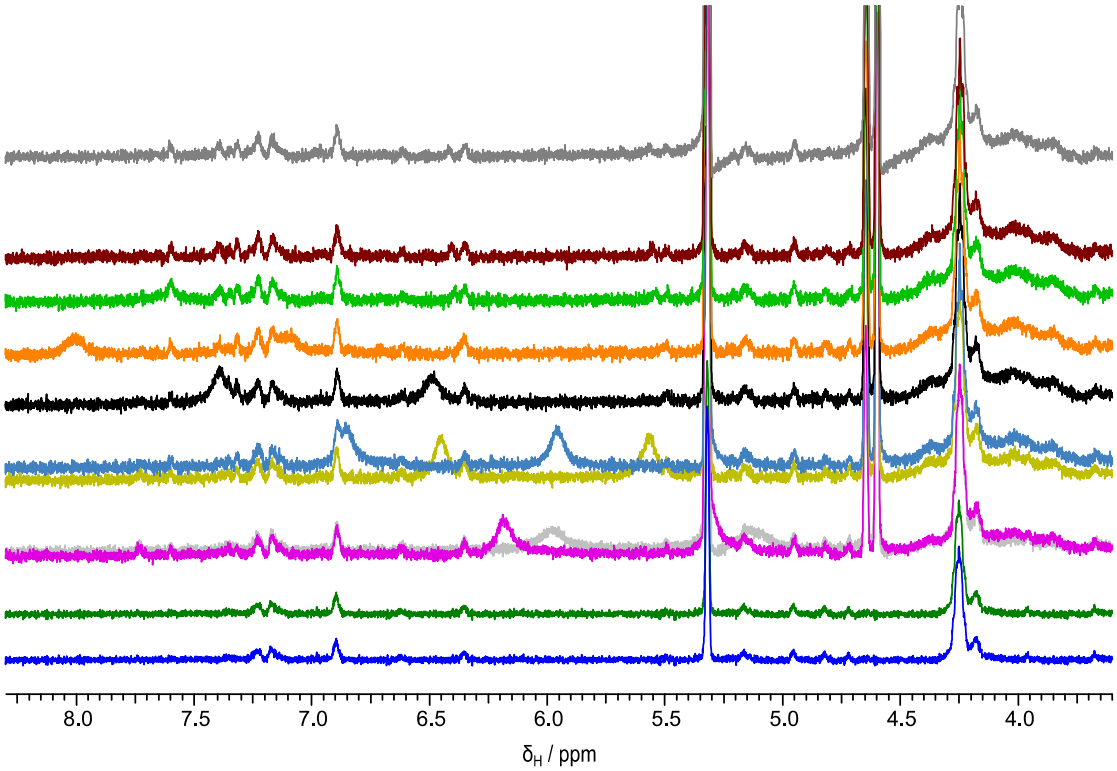

Figure S13a ^{1}H NMR spectra showing the progress of H_2 cleavage by the **8**/P(^{t}Bu)$_3$ FLP post H_2 addition spectra at *ca.* 12 hour intervals

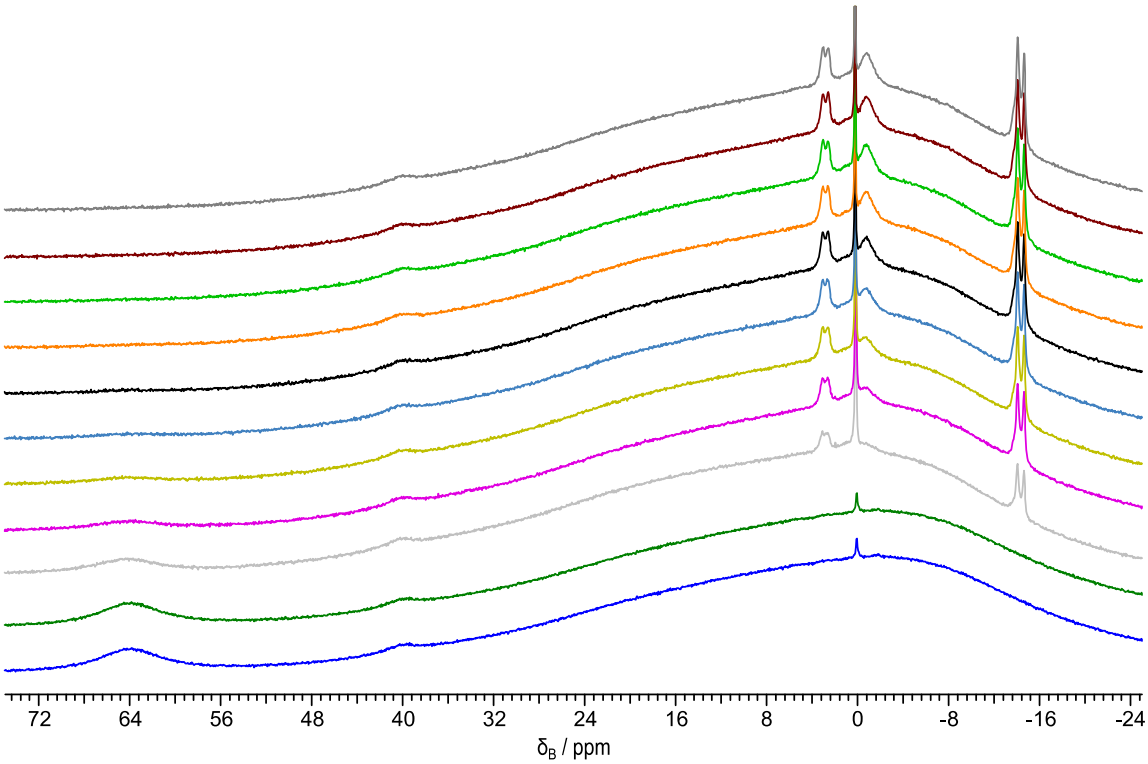

Figure S13b ^{11}B NMR spectra showing the progress of H_2 cleavage by the **8**/P(^{t}Bu)$_3$ FLP post H_2 addition spectra at *ca.* 12 hour intervals

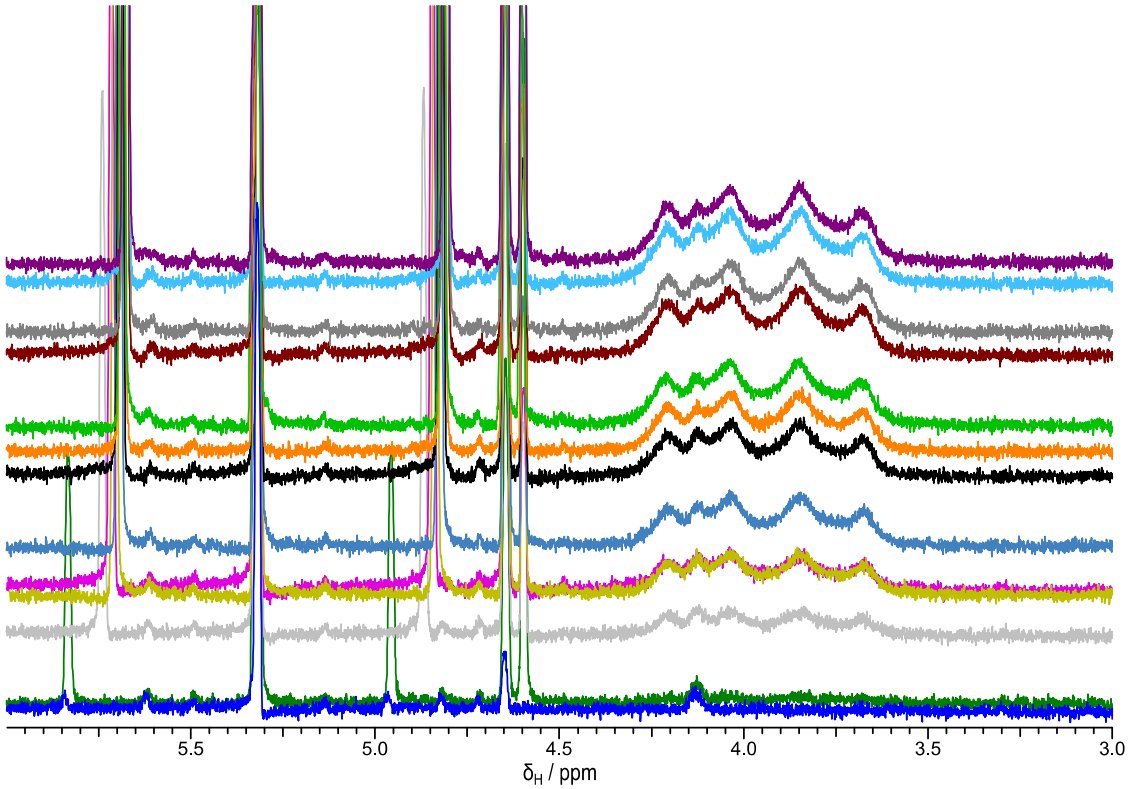

Figure S14a ^{1}H NMR spectra showing the progress of H_2 cleavage by the **9**/P(^{t}Bu)$_3$ FLP post H_2 addition spectra at *ca.* 90 min intervals

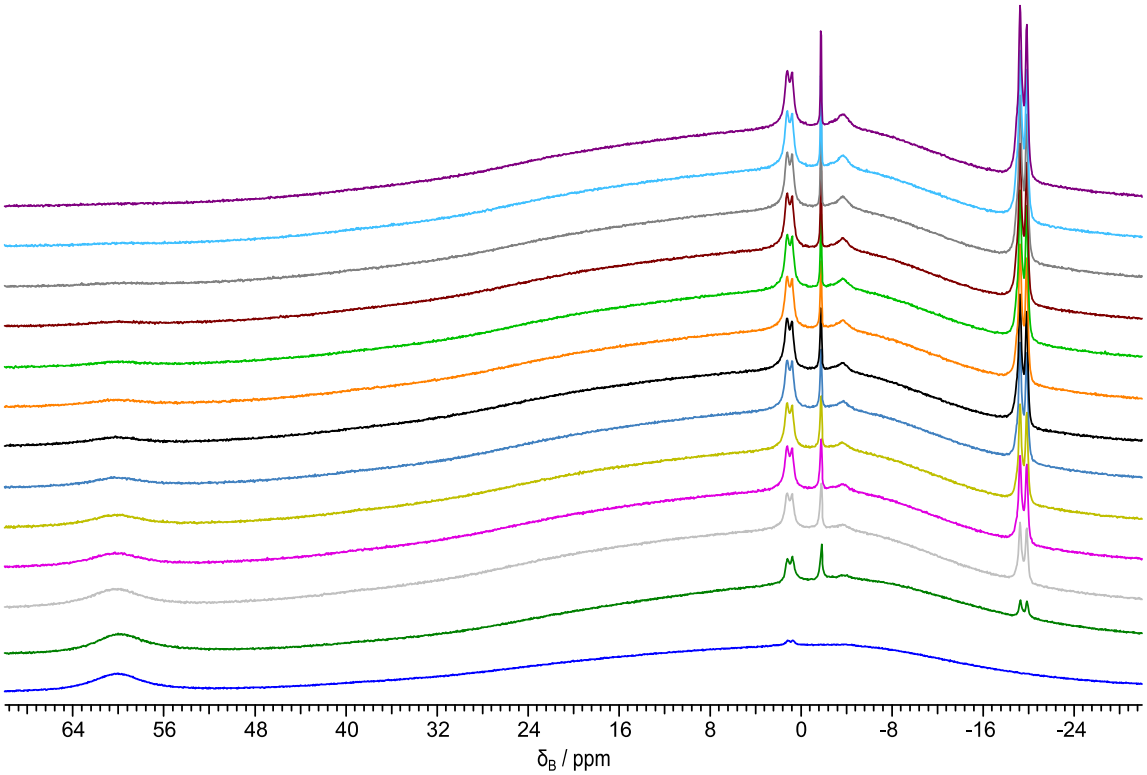

Figure S14b ^{11}B NMR spectra showing the progress of H_2 cleavage by the **9**/P(^{t}Bu)$_3$ FLP post H_2 addition spectra at *ca.* 90 min intervals